Waveforms of Langmuir turbulence in inhomogeneous solar wind plasmas

C Krafft, A. Volokitin, V.V. Krasnoselskikh, Thierry Dudok de Wit

AGU PUBLICATIONS

JGR

Journal of Geophysical Research: Space Physics

RESEARCH ARTICLE

10.1002/2014JA020329

Key Points:
- Simulations of Langmuir turbulence in the solar wind
- Langmuir waveforms
- Comparison with STEREO and WIND observations

Correspondence to:
C. Krafft,
catherine.krafft@lpp.polytechnique.fr

Citation:
Krafft, C., A. S. Volokitin, V. V. Krasnoselskikh, and T. Dudok de Wit (2014), Waveforms of Langmuir turbulence in inhomogeneous solar wind plasmas, *J. Geophys. Res. Space Physics*, *119*, 9369–9382, doi:10.1002/2014JA020329.

Received 24 JUN 2014
Accepted 5 NOV 2014
Accepted article online 8 NOV 2014
Published online 16 DEC 2014

Waveforms of Langmuir turbulence in inhomogeneous solar wind plasmas

C. Krafft[1,2], A. S. Volokitin[3,4], V. V. Krasnoselskikh[5], and T. Dudok de Wit[5]

[1]Laboratoire de Physique des Plasmas, Ecole Polytechnique, Palaiseau, France, [2]Laboratoire de Physique des Plasmas, Ecole Polytechnique, Palaiseau, Paris XI - Paris Sud University, Orsay, France, [3]Space Research Institute, Moscow, Russia, [4]IZMIRAN, Moscow, Russia, [5]Laboratoire de Physique et Chimie de l'Environnement et de l'Espace, Orléans, France

Abstract Modulated Langmuir waveforms have been observed by several spacecraft in various regions of the heliosphere, such as the solar wind, the electron foreshock, the magnetotail, or the auroral ionosphere. Many observations revealed the bursty nature of these waves, which appear to be highly modulated, localized, and clumped into spikes with peak amplitudes typically 3 orders of magnitude above the mean. The paper presents Langmuir waveforms calculated using a Hamiltonian model describing self-consistently the resonant interaction of an electron beam with Langmuir wave packets in a plasma with random density fluctuations. These waveforms, obtained for different profiles of density fluctuations and ranges of parameters relevant to solar type III electron beams and plasmas measured at 1 AU, are presented in the form they would appear if recorded by a satellite moving in the solar wind. Comparison with recent measurements by the *STEREO* and *WIND* satellites shows that their characteristic features are very similar to the observations.

1. Introduction

During the last decades, modulated Langmuir waveforms have been observed in various regions of the heliosphere such as the electron foreshock, the solar wind, the magnetotail, or the auroral ionosphere [e.g., *Gurnett et al.*, 1993; *Kojima et al.*, 1997; *Bonnell et al.*, 1997; *Kellogg et al.*, 1999; *Souček et al.*, 2005, and references therein]. In particular, modulated Langmuir waves associated with type III solar bursts were measured in the solar wind by many satellites as *ISEE 1–3*, *Helios, Voyager, Galileo, Ulysses, Geotail, Wind, Cluster*, and *STEREO* [e.g. *Gurnett and Anderson*, 1976; *Lin et al.*, 1981; *Gurnett et al.*, 1992; *Ergun et al.*, 1998; *Mangeney et al.*, 1999; *Kellogg et al.*, 2009; *Hess et al.*, 2011, and references therein]. They are thought to be generated by streams of high-energy electrons accelerated in the solar corona during flares via beam instability and converted into electromagnetic radiation near f_p and $2f_p$ via nonlinear processes [*Ginzburg and Zheleznyakov*, 1958]. Many observations revealed the bursty nature of these highly modulated and clumped wave packets. They were first registered by the Helios spacecraft between 0.3 and 1 AU [e.g., *Gurnett and Anderson*, 1976]; further many measurements were performed by other satellites, revealing more intense Langmuir waveforms, with electric field peaks reaching from 10^2 to 10^3 times the mean [e.g., *Gurnett et al.*, 1978; *Lin et al.*, 1986; *Nulsen et al.*, 2007; *Gurnett et al.*, 1993; *Ergun et al.*, 2008; *Malaspina et al.*, 2010]. In particular, recent in situ high time resolution observations by the *Time Domain Sampler* (*TDS*) instrument [*Bougeret et al.*, 2008] onboard the STEREO (*Solar TErrestrial RElations Observatory*) satellite show that they often appear as intense and clumpy packets with durations of few milliseconds and electric field amplitudes up to a few tens of mV/m [*Malaspina et al.*, 2010, 2011; *Hess et al.*, 2011]. With registration times from 65 ms to 2 s [*Bougeret et al.*, 2008], the STEREO/TDS instrument can capture a great amount of wave packets with typical scales around several hundreds of electron Debye lengths, resolving structures on the scale of 10 m. Durations of waveforms' registration are roughly 10 times longer than onboard the previous missions. Note that they appear mostly as multiple bursts' events, which are much more frequently observed than more isolated and well-shaped structures exhibiting one or a few humps.

The ISEE 1–2 spacecraft [*Celnikier et al.*, 1983] showed that average levels of density fluctuations exceeding 1% of the background plasma density and extending on scales around 100 km likely exist in the solar wind. In particular, it was found [*Celnikier et al.*, 1983, 1987] that the power spectrum of the electron density follows two power laws, one in the higher-frequency range above 0.1 Hz and the other one below. Moreover, spectra of rapid density fluctuations were obtained using the *EFW* (*Electric Field and Waves Experiment*)

probe potential variations measured by the Cluster mission in the solar wind [*Kellogg and Horbury*, 2005]. More recently, *Ergun et al.* [2008] and *Krasnoselskikh et al.* [2007] have reported direct observations in the solar wind of unusually large levels of density fluctuations. Thus, the well-known theory of beam-plasma interaction developed for homogeneous plasmas cannot be applied to such cases, and the models have therefore to take into account from the very beginning the effects due to large-amplitude randomly varying density fluctuations.

Then, the presence of fluctuating inhomogeneities of finite sizes and depths in the solar wind where modulated and localized Langmuir bursts are commonly observed leads to address several important questions. Indeed, the physical processes responsible for such wave packets' modulations have to be explained, and the influence of the resulting clumped structures on the propagation and the growth of the waves as well as on their eventual conversion into electromagnetic radiation have to be elucidated. Many models have been proposed up to now. In particular, it was argued that the solar wind density inhomogeneities may be responsible for such phenomena, including effects of refraction, reflection, and scattering of plasmons by density fluctuations, or also stochastic growth effects [*Robinson*, 1992]. Analyzing plasmons in type III solar bursts, *Smith and Sime* [1979] showed that density inhomogeneities can significantly influence on the growth of waves that follow slightly different paths when crossing the amplification regions; they proposed that the formation of clumpy structures should be due to the strong decrease of the bump-on-tail instability by density fluctuations of sizes of the order of the waves' spatial growth rates. Then waves can be amplified only along the paths where the encountered inhomogeneities are sufficiently similar not to perturb the amplification processes leading to the formation of spikes. This idea was further developed by several authors [e.g., *Melrose et al.*, 1986; *Kellogg*, 1986; *Robinson*, 1992; *Boshuizen et al.*, 2004; *Robinson et al.*, 1993]. Moreover, recent numerical simulations using the Zakharov equations [*Zakharov*, 1972] have found that Langmuir waves excited by beams in plasmas with randomly varying density inhomogeneities of finite amplitude exhibit such clumpy structures with characteristics very close to those revealed by the most recent observations [*Krafft et al.*, 2013; *Volokitin et al.*, 2013]. Other processes, as trapping of waves in density fluctuations, have also been proposed by some authors [*Malaspina and Ergun*, 2008; *Ergun et al.*, 2008; *Zaslavsky et al.*, 2010] who explain that the Langmuir waveforms should be eigenmodes of density cavities resulting from plasma turbulence. Moreover, various mechanisms have been discussed, among which weak turbulence processes such as electrostatic decay [e.g., *Lin et al.*, 1986; *Hospodarsky and Gurnett*, 1995; *Henri et al.*, 2009; *Thejappa et al.*, 2003], kinetic localization [*Muschietti et al.*, 1994, 1995], or strong turbulence processes as modulational instabilities or collapse [*Nicholson et al.*, 1978; *Thejappa et al.*, 2003]. However, no consensus has been reached yet to explain the mechanisms responsible for the clumpy and modulated nature of solar type III Langmuir waveforms and for their further radiation in electromagnetic emission.

This paper presents typical Langmuir waveforms calculated using a Hamiltonian model which describes the self-consistent resonant interactions between electron beams and Langmuir waves in plasmas with randomly varying density fluctuations. The waveforms obtained for different profiles of density fluctuations as well as for beam and plasma parameters relevant to type III solar bursts' characteristics at 1 AU [e.g., *Ergun et al.*, 1998] are compared with recent measurements by the STEREO and Wind spacecraft, showing that the bursty localized structures characterizing the waveforms are very similar to the observations. The model is based on the Zakharov's equations, where a source term is added to describe the electron beam; it also includes the low-frequency response of the plasma (with ponderomotive force effects) and the presence at the initial state of strong and random density inhomogeneities (up to 5% of the background density). Let us stress that the density fluctuations considered here are not resulting from strong turbulence effects but are imposed initially. The beam is described by means of a particle-in-cell (PIC) code, but, unlike the usual PIC approaches where the numerical noise can be reduced by the high number of particles used, the present model divides the particle velocity distribution in two groups: (i) the plasma background whose particles interact nonresonantly with the waves and (ii) the beam particles which exchange resonantly significant amounts of energy and momentum with the waves [e.g., *O'Neil et al.*, 1971; *Zaslavsky et al.*, 2006; *Volokitin and Krafft*, 2004]. Then the motion of the beam (resonant) particles only is calculated by solving the Newton equations. The background particles support the waves' dispersion, and their dynamics is modeled using the dielectric constant in the frame of a linear analysis. Such approach leads to a drastic reduction of the number of macroparticles required in the calculations and thus allows to follow their dynamics during large lapses of time [e.g., *Volokitin and Krafft*, 2012].

The waveforms calculated by the simulations represent the profiles of the electric field envelope as a function of the spatial coordinate z along the 1-D simulation box (note that the observed Langmuir wavefields are mainly linearly polarized along the magnetic field lines [*Ergun et al.*, 2008]). In order to compare them with the observed waveforms as those captured by STEREO (*stereo.gsfc.nasa.gov*) and presented by several authors [e.g., *Gurnett et al.*, 1981; *Kellogg et al.*, 1999; *Ergun et al.*, 2008; *Henri et al.*, 2009; *Malaspina et al.*, 2010, 2011; *Graham et al.*, 2012; *Graham and Cairns*, 2013a; *Graham and Cairns*, 2013b], we present them as they would appear if recorded by a spacecraft moving with a velocity v_S in the flowing solar wind. Indeed, the waveforms observed in the satellite's frame are Doppler shifted as the plasma is moving at the solar wind speed $V_{SW} \simeq$ 200–800 km/s. Note that, in order to perform meaningful comparisons between simulated and observed waveforms, we consider only wave packets at the stage when the beam instability is saturated.

2. Numerical Simulations

The simulation results presented below are based on the 1-D Zakharov equations [*Zakharov*, 1972] and describe the evolution of the slowly varying envelope $E(z,t) = \sum_k E_k(t)e^{ikz}$ of the Langmuir wave electric field $\mathcal{E}(z,t) = E(z,t)e^{-i\omega_p t}$ + c.c. in a background plasma with initial long-wavelength random density fluctuations δn of average level $\Delta n = \left\langle (\delta n/n_0)^2 \right\rangle^{1/2}$; E_k, k, and ω_p are the Fourier component of E, the wave vector, and the electron plasma frequency; n_0 is the background plasma average density. The mathematical model (see *Krafft et al.* [2013] and Appendix A) includes an additional term in the high-frequency Zakharov equation which represents the contribution of the electron beam. The second Zakharov equation for the low-frequency dynamics contains all ponderomotive force effects. The variables are normalized as $\omega_p t$, z/λ_D, v/v_T, and $E_k/\sqrt{4\pi n_0 T_e}$; then the dimensionless wave energy density (or level of turbulence) is $|E|^2/4\pi n_0 T_e$; λ_D, v_T, and T_e are the electron Debye length, thermal velocity, and temperature of the background plasma.

A classical leapfrog scheme is used for the integration of the electron motion (A3). The differential equations (A4)–(A6) describing the evolution of the Fourier components of the electric field, E_k, of the plasma density, $\rho_k = (\delta n/n_0)_k$, and of the ion velocity, u_k, are solved owing to discrete time approximations and fast Fourier transforms' algorithms. The boundary conditions are periodic. The length of the system is $L \simeq 10,000$–$30,000\lambda_D$; the beam electrons travel along this simulation box during a time lapse of the order of or smaller than the simulation time. Initially, 1024–2048 plasma waves of random phases and small amplitudes are distributed in the Fourier space, with wave vectors $-k_{max} < k < k_{max}$, where $k_{max}\lambda_D \simeq$ 0.2–0.3 and $\delta k\ \lambda_D \simeq$ 0.0004–0.0006; δk is the spectral width between two neighbor wave modes. Thermal damping is not considered here, as waves interacting with the background plasma (i.e., of phase velocities $\omega_k/k \lesssim 3v_T$) satisfy $k\lambda_D \gtrsim 0.3$. The beam distribution is modeled by a Maxwellian function of average and thermal velocities v_b and Δv_b, respectively; initially the resonant electrons are distributed uniformly in space.

Calculations are performed for parameters typical for solar type III plasmas and beams at 1 AU [e.g., *Ergun et al.*, 1998]; then we have $c/20 \lesssim v_b \lesssim c/3$ and $0.05 \lesssim \Delta v_b/v_b \lesssim 0.1$. The ambient plasma density and temperature are roughly $n_0 \simeq 5\ 10^6$ m^{-3} ($\omega_p/2\pi \simeq 20$ kHz) and $T_e \simeq$ 10–20 eV; note that $\lambda_D \sim 15$ m. The background plasma density is much larger than the beam density, i.e., $5\ 10^{-6} \lesssim n_b/n_0 \lesssim 5\ 10^{-5} \ll 1$. Initially, the average level of density inhomogeneities is around $0.001 \lesssim \Delta n \lesssim 0.05$, and the density perturbation profiles $\delta n(z)/n_0$ present spatial scales around $300 \lesssim \lambda_n \lesssim 2000\lambda_D$ much above the plasmons' wavelengths. For such parameters, the condition required for bump-on-tail kinetic instability is fulfilled, i.e., $\left(n_b/n_0\right)^{1/3} \lesssim \Delta v_b/v$. Finally, the level of turbulence in our simulations does not exceed the thresholds of modulational instability, collapse, or strong ponderomotive effects.

In our previous works [*Zaslavsky et al.*, 2010; *Krafft et al.*, 2013; *Volokitin et al.*, 2013], the impact of the background density fluctuations on the electron beam dynamics and the Langmuir spectrum's evolution was studied. In this view, we present below several relevant examples of Langmuir waveforms exhibiting wave modulation and focusing effects in order to compare them with observations by the spacecraft STEREO and Wind. Here one has to take into consideration the time Δt during which a wave packet crosses the moving satellite. A Langmuir packet is propagating with a group velocity of the order of $v_g/v_T \sim 3k\lambda_D \sim$ 0.15–0.3; the solar wind velocity is around $V_{SW} = |\mathbf{V}_{SW}| \simeq$ 200–800 km/s (i.e., $V_{SW} \simeq$ 0.1–0.6 v_T for $T_e \sim$ 10–20 eV), so that the satellite velocity in the solar wind frame is $\mathbf{v}_S \simeq -\mathbf{V}_{SW}$ (it is neglected in the laboratory frame); so the relative velocity between the Langmuir packet and the satellite is $\mathbf{v}_r \simeq \mathbf{v}_g + \mathbf{V}_{SW}$, that is, $v_r = |\mathbf{v}_r| \simeq$ 0.2–0.9v_T. Note that below we use the notation $v_S = |\mathbf{v}_S| \simeq |\mathbf{V}_{SW}|$. Then, the time Δt during which a wave packet of width Δz crosses the satellite is roughly $\Delta z/v_r$; typically, for wave packets of sizes of the order of

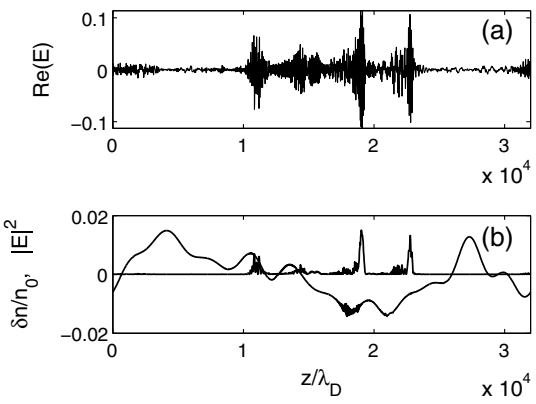

Figure 1. (a and b) Profiles of the electric field envelope E, the wave energy density $|E|^2$, and the density perturbations $\delta n/n_0$ at $\omega_p t = 30,000$. Main parameters are the following: $n_b/n_0 = 2\ 10^{-5}$, $v_b = 18 v_T$, $\Delta n \simeq 0.01$, and $L = 32,000\lambda_D$.

2000–5000λ_D, Δt is around (0.3–3) $10^4\omega_p^{-1}$. According to our simulations, the profiles of the wave packets can be significantly changed and even totally destroyed during such time scale. We present below several examples showing the differences between the spatial profiles of the electric field envelopes at some given times (i.e., calculated by our simulations in the solar wind frame and so-called "instantaneous" waveforms) and the corresponding waveforms that would be observed by a satellite starting from the same time at the position z_S and moving with the relative velocity v_r across the Langmuir packet. The electric field which would be measured on the spacecraft is calculated according to $E_S(t) = \mathrm{Re}\sum_k E_k(t) \exp(ik(z - v_S t) - i\omega_p t)$. Then the temporal modulation patterns obtained result from the convection of the spatial Langmuir structures across the satellite by the solar wind flows. The corresponding waveforms—the so-called "observed" waveforms—show, even in the case of very small inhomogeneities, spatial modulations of different scales.

The variations of the field envelope profiles are very fast in the initial stage of the beam relaxation and may not well correspond to what is actually observed after a longtime propagation of the beam. We study hereafter the stage when the wave saturation is achieved and the beam relaxation process is well advanced. At this stage the velocity distribution $f(v)$ presents a plateau with a more or less small gradient $\partial f/\partial v \gtrsim 0$. An overview of the Langmuir turbulence at this stage is shown in Figures 1–4. The first figure presents the electric field envelopes' profiles $E(z)$, the wave energy density $|E|^2$ (or level of turbulence), and the density fluctuations $\delta n/n_0$ at time $\omega_p t = 30,000$, when the total spectral energy density $W = \sum_k |E_k|^2$ saturates (Figure 3a) and the beam is almost fully relaxed (Figure 3b). The time evolution of $f(v)$ in Figure 3b shows that the beam distribution broadens and diffuses to lower velocities, whereas a tail of accelerated particles appears at velocities $v \gtrsim v_b$. Meanwhile, W grows (Figure 3a), reaching slowly saturation, which is fully achieved when the beam decelerating velocity front has reached the thermal domain at $v \lesssim 3v_T$. One can observe in Figure 1 that the plasmon energy density $|E|^2$ is concentrated in a few well-localized packets (Figure 1b) which, once formed, propagate with a roughly constant velocity but experience significant modifications in shape and amplitude, as shown by the variation with time of the wave energy profile (Figure 2). To complete the dynamics of the system, Figure 4 presents the high- and low-frequency spectra at $\omega_p t = 30,000$; one observes that the high-frequency spectrum peaks near $k_b\lambda_D = v_T/v_b \simeq 0.055$, which is the wave number at the Landau resonance condition; it is broadened due to scattering and reflections of Langmuir waves on the density inhomogeneities, as shown by the presence of counterpropagating waves with $k < 0$ (see also Figure 4). The low-frequency spectrum reveals noise with rather broad peaks which possibly indicate the presence of wave-wave coupling and electrostatic decay, which is related to the peak near $k\lambda_D \simeq -0.05$ in the Langmuir spectrum of Figure 4a. The role of these processes will be considered in a forthcoming paper. Figures 1–4 correspond to a global view of the system, i.e., including the

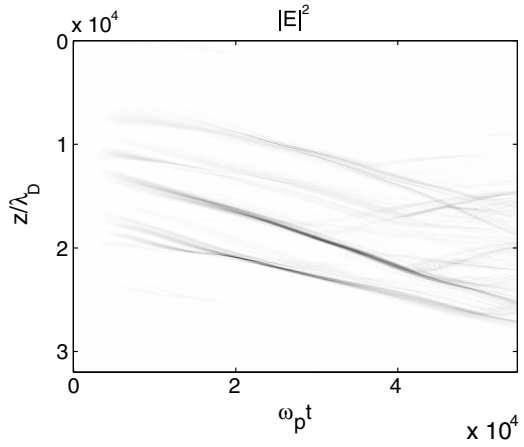

Figure 2. Profile of the wave energy $|E|^2(z,t)$ as a function of time $\omega_p t$ and space z/λ_D. Parameters are the same as in Figure 1.

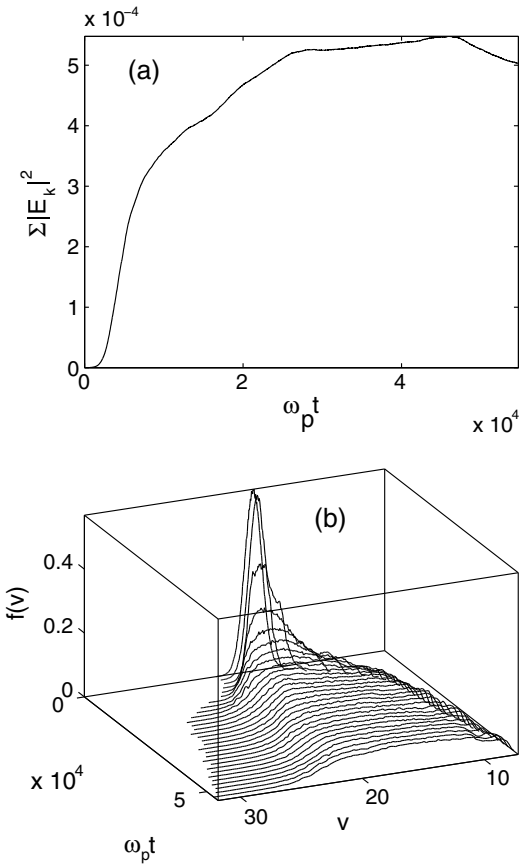

Figure 3. Time evolution up to $\omega_p t = 54,000$ of (a) the total wave energy density $W = \sum_k |E_k|^2$ and (b) the electron beam velocity distribution $f(v)$ (v is normalized by v_T). Parameters are the same as in Figure 1.

evolution of all wave packets propagating over the whole length of the simulation box. Note that the amplitude of the Langmuir turbulence is small ($|E|^2 \lesssim 0.01$) and, correspondingly, that the ponderomotive forces are weak and that no cavity (density depletion) is formed in the plasma.

In the figures presented below, only local processes are studied, i.e., one only examines instantaneous wave packets where wave-wave interaction processes involving ion-sound waves are very slow and do not play a significant role. This means that we study the time evolution of some chosen part of the simulation box where we select instantaneous wave packets which are not influenced by nonlinear effects due to wave-wave coupling or modulational instability, for example. The profiles of the field envelopes calculated during the simulations at times $\omega_p t = 13,000$ and $\omega_p t = 25,000$ within the window $[L_{\min}, L_{\max}] = [5000, 22,000]$ are shown in Figures 5a and 5b for physical parameters close to those of Figures 1–4. One can observe the presence of roughly four Langmuir wave packets at $\omega_p t = 13,000$, which keep more or less their identity during their propagation until $\omega_p t = 25,000$, in spite of noticeable variations of their forms. Figures 5c and 5d show the corresponding waveforms that would be observed onboard a spacecraft moving relatively to the solar wind with the velocities $v_S = 0.2v_T$ and $v_S = 0.6v_T$, respectively, supposing that the observation starts when the satellite is located at the position $z_S = 16,000\lambda_D$ (indicated by an upward vertical line in Figure 5a) and finishes when it arrives at $z = 13,600\lambda_D$ or at $z = 8800\lambda_D$, for $v_S = 0.2v_T$ and $v_S = 0.6v_T$, respectively (the final positions are indicated by downward lines in Figure 5a). Both waveforms in Figures 5c and 5d reveal clumpy features with beatings, which are typical of STEREO records; the waveform observed at $v_S = 0.2v_T$ (Figure 5c) corresponds roughly to the part of the waveform at $v_S = 0.6v_T$ (Figure 5d) extending from $t \simeq 13,000\omega_p^{-1}$ up to $t \simeq 18,000\omega_p^{-1}$. So it appears that the variation of the satellite velocity—i.e., of the solar wind speed or of its temperature—does not modify strongly the appearance of the successive clumps of the waveform (that obviously is not the case for the initial satellite position and the initial observation time). Note that, for lower satellite velocities, fine structures as beatings, for example, appear more clearly, with a better resolution. Then, some remarks can be formulated. First, the observed waveforms (Figures 5c and 5d) differ noticeably from the instantaneous ones (Figures 5a and 5b), what clearly corresponds to the modification of the wave packets' profiles during the time of observation. Second, the features of the observed waveforms depend significantly on the spacecraft's initial location, but a significant variation of the satellite velocity does not distort the registration of the wave packets. However, this is true only if the wave packets propagate rather stably during the observation time; if they are strongly modified by nonlinear effects during the observation time, this last conclusion may become false and a variation of v_S can modify essentially the main features of the waveform. Third, the observed waveforms present characteristics similar to those recorded in the solar wind by the Wind and STEREO spacecraft (see, for example, and among others, *Malaspina et al.* [2010, Figure 1b] and *Malaspina et al.* [2011, Figure 2a]).

For the same parameters and the same train of Langmuir packets as in Figures 5a–5d, but for a different time of observation and satellite location—with the same spacecraft velocity $v_S = 0.6v_T$—one observes

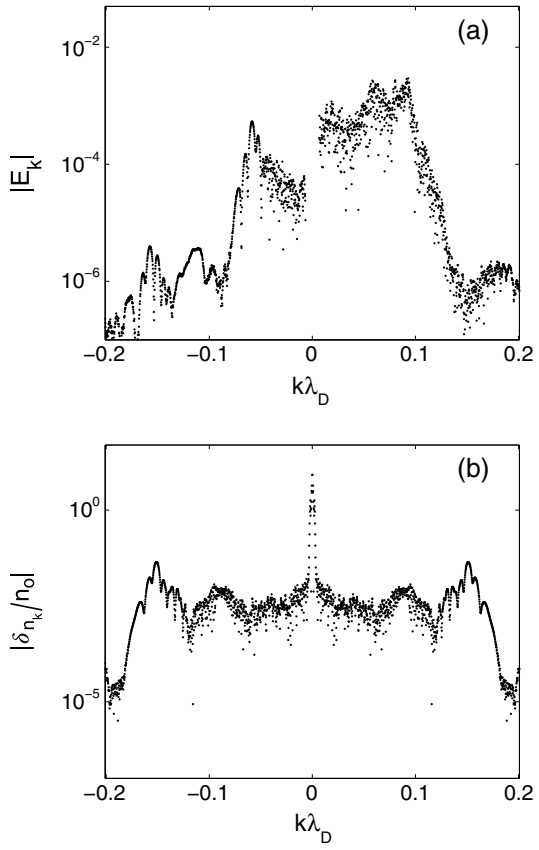

Figure 4. Spectra at $\omega_p t = 30,000$ and in logarithmic scale of (a) the Langmuir waves and (b) the low-frequency density fluctuations; E_k and $\delta n_k/n_0$ are the Fourier components of E and $\delta n/n_0$. Parameters are the same as in Figure 1.

a totally different picture, as revealed by Figure 6a which shows an observed waveform appearing as an isolated packet containing a quasi-symmetric modulation pattern. Such structures have been observed, for example, by *Ergun et al.* [2008, Figure 3a], *Graham and Cairns* [2013b, Figure 8a], and *Henri et al.* [2009, Figure 3c]. Note also that for the case of type III solar bursts, the Langmuir waves are propagating in the solar wind flow direction. At the foreshock, Langmuir waves propagate opposite to the solar wind; then, the spacecraft velocity in the solar wind frame is $\mathbf{v}_S \simeq \mathbf{V}_{SW}$, but its modulus lies roughly within the same range of v_S values as used above. Conclusions concerning the influence of the satellite velocity variation on the waveforms are similar as for the case of type III solar bursts.

Note that in most cases the solar wind flow and the ambient magnetic field are not aligned, as supposed in the present 1-D study. However, if one can neglect the component of the electric field $E_\perp$ perpendicular to the magnetic field with respect to the parallel one E_z, as it is possible for around 70% of the events, a nonvanishing angle θ between the magnetic field and the solar wind flow will only have an incidence on the satellite velocity, whose absolute value should decrease when θ increases. Figure 6b shows the observed waveform calculated for the

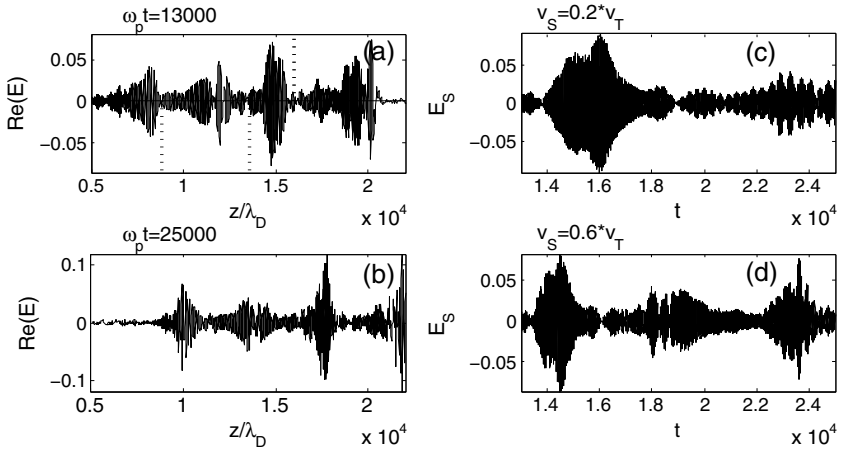

Figure 5. (a and b) Instantaneous electric field spatial profiles at times $\omega_p t = 13,000$ and $\omega_p t = 25,000$, within the subbox $[L_{\min}, L_{\max}] = [5000, 22, 000]$. (c and d) Corresponding waveforms which would be observed by a satellite moving at velocity $\mathbf{v}_S$ (of modulus v_S) and starting at $z_S = 16,000\lambda_D$ at time $\omega_p t = 13,000$; the position z_S is indicated by an upward dotted vertical line in Figure 5a; the final positions of the satellite moving at the velocities $v_S = 0.2v_T$ (Figure 5c) and $v_S = 0.6v_T$ (Figure 5d) are marked by downward dotted vertical lines in Figure 5a; E_S is the electric field amplitude measured by the virtual spacecraft (normalized as the field E), and t is the time in units of ω_p^{-1}. Physical parameters are the same as in Figure 1.

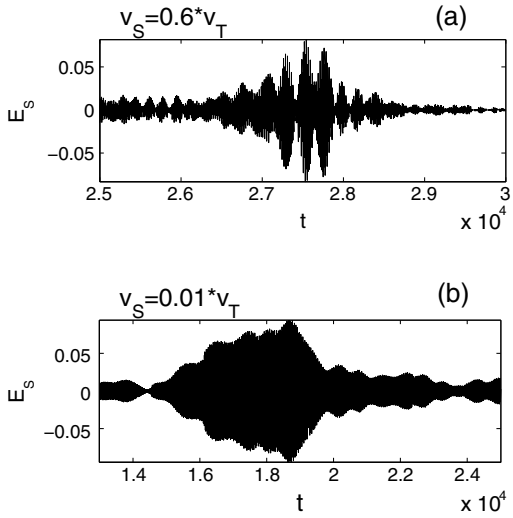

Figure 6. (a) Waveform observed at $v_S = 0.6v_T$ for the same conditions as in Figures 5a–5d but with $25,000 < \omega_p t < 30,000$ and $z_S = 12,000\lambda_D$. (b) Waveform observed for the same conditions as in Figures 5a–5d but for $v_S = 0.01v_T$. Physical parameters are the same as in Figure 1.

same conditions as in Figure 5, but for a much smaller velocity $v_S = 0.01v_T$. The same qualitative observations can be provided: even a significant decrease of the satellite velocity does not distort the recorded waveform. On the other hand, if the perpendicular component of the electric field cannot be neglected, we have to take care that, during its observation time Δt, the satellite should travel within the perpendicular spatial extent $l_\perp$ of the wave packet. Taking into account that the length l_z of the Langmuir packet along the magnetic field is typically around 10 km and that, according to the fact that waves are quasi-potential, we have $E_z/E_\perp \sim l_\perp/l_z$ with, for 70% of cases, $E_z/E_\perp \sim 10$ or less (i.e., $l_\perp \sim 10 l_z$ or more), the above condition can be written as $|V_{SW} \sin\theta|\ \Delta t \ll 10 l_z$, which gives for typical values ($V_{SW} \sim 500$ km/s, $\Delta t \sim 0.05$ s, $l_z \sim 10$ km) that $|\sin\theta| \ll 4$, condition which is always fulfilled. In all such cases, our 1-D modeling can thus be applied. When the ratio $E_z/E_\perp$ is smaller and the perpendicular field component cannot be neglected, i.e., $E_z/E_\perp \sim 3$, the condition is $|\sin\theta| \ll 1$, which continues to be true if θ is roughly less than 20°.

A next example is shown by Figure 7 for a denser beam, which presents in the same form as Figure 5 two instantaneous with their corresponding observed waveforms, for the velocities $v_S = 0.3v_T$ and $v_S = 0.6v_T$, respectively. The same remarks can be done as above for Figure 5. Moreover, the observed waveform for $v_S = 0.6v_T$ (and also $v_S \gtrsim 0.6v_T$) reproduces more or less accurately the structures of the instantaneous wave packets (compare the instantaneous wave packets between $z = 7000\lambda_D$ and $z \simeq 20,000\lambda_D$ with the observed wave packets between $\omega_p t \simeq 18,000$ and $\omega_p t \simeq 30,000$). Structures revealed by these waveforms resemble to the observations reported, for example, by *Graham and Cairns* [2013b, Figure 19a] and *Gurnett et al.* [1981, Figure 7b].

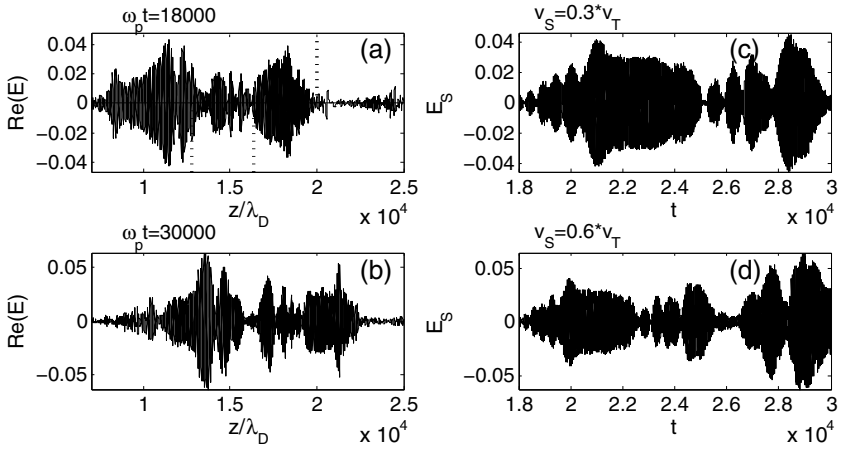

Figure 7. (a and b) Instantaneous electric field profiles at times $\omega_p t = 18,000$ and $t = 30,000$, within the subbox $[L_{\min}, L_{\max}] = [7000, 25, 000]$. (c and d) Corresponding waveforms which would be observed by a satellite moving at velocity v_S and starting at $z_S = 20,000\lambda_D$ at time $\omega_p t = 18,000$; the position z_S is indicated by an upward dotted vertical line in Figure 7a; the final positions of the virtual satellite moving at the velocities $v_S = 0.3v_T$ (Figure 7c) and $v_S = 0.6v_T$ (Figure 7d) are marked by downward dotted vertical lines in Figure 7a. Main parameters are the following: $n_b/n_0 = 5\ 10^{-5}$, $v_b = 18v_T$, and $\Delta n \simeq 0.01$.

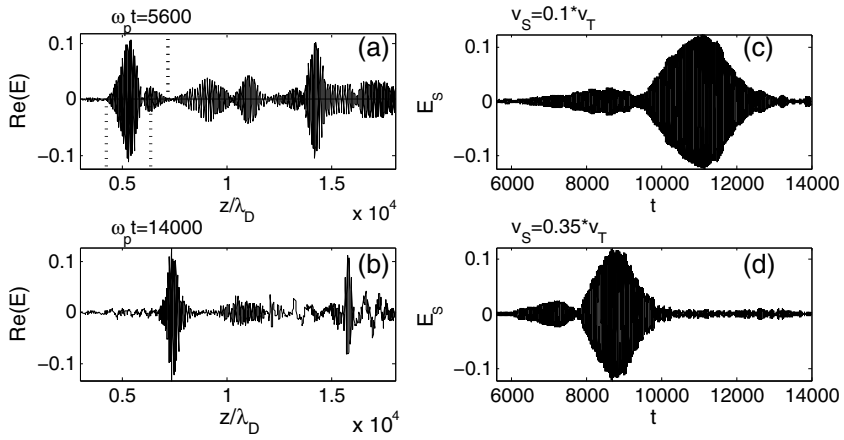

Figure 8. (a and b) Instantaneous electric field profiles at times $\omega_p t = 5600$ and $\omega_p t = 14,000$, in the subbox $[L_{\min}, L_{\max}] = [3000, 18, 000]$. (c and d) Corresponding waveforms which would be observed by a satellite moving at velocity v_S and starting at $z_S = 7200\lambda_D$ (upward dotted vertical line in Figure 8a) at time $\omega_p t = 5600$; the final positions of the satellite moving at the velocities $v_S = 0.1v_T$ (Figure 8c) and $v_S = 0.35v_T$ (Figure 8d) are marked by downward dotted vertical lines in Figure 8a. Main parameters are the following: $n_b/n_0 = 10^{-5}$, $v_b = 18v_T$, and $\Delta n \simeq 0.01$.

Figures 8a and 8b show a localized instantaneous packet which stably propagates during a long time interval after it was formed (near $z \simeq 5000\lambda_D$ for $\omega_p t = 5600$ (a) and $z \simeq 7000\lambda_D$ for $\omega_p t = 14,000$ (b)). The corresponding observed waveforms calculated for $v_S \simeq 0.1v_T$ (c) and $v_S \simeq 0.35v_T$ (d) present strong similarities and show isolated wave packets as those presented in *Ergun et al.* [2008, Figure 1a], *Graham et al.* [2012, Figure 2a], *Graham and Cairns* [2012, Figure 2a], or *Gurnett et al.* [1981, Figure 7a], which were interpreted by the authors as possible trapped or collapsing wave packets. These isolated structures remain very stable when the satellite velocity is modified. However, for the same physical parameters and for $v_S \simeq 0.6v_T$, but changing only the conditions of observation (duration, initial satellite position, and starting time), one observes totally different waveforms, as shown in Figure 9 which exhibits regular beatings, similar to space observations reported by some authors [*Graham and Cairns*, 2013b, Figure 6a; *Gurnett et al.*, 1981, Figure 3].

Isolated clumps are not easily observed in our simulations in the presence of very weak ($\Delta n \sim 0.001 \ll 0.01$) or of too high ($\Delta n \gtrsim 0.03$) density fluctuations; therefore, they likely could be a signature of the presence of fluctuations with $\Delta n \sim 0.01$. Note also that, if plasma waves propagate in the direction opposite to the solar wind flow, isolated packets are no more observed and trains of modulated packets are present instead.

Moreover, we can guess that it becomes possible to speak about the "observation" of isolated wave packets only if the average level Δn of the background density fluctuations exceeds some threshold. To support this, one presents in Figure 10 two examples of typical instantaneous profiles obtained for $\Delta n \simeq 0.001$. Typically, in all our simulations with $\Delta n \ll 0.01$, it was very difficult if not possible to find isolated packets in the instantaneous field envelope profiles. For a satellite velocity $v_S \simeq 0.1v_T$, the corresponding observed waveform, which can be compared, for example, to *Kellogg et al.* [1999, Figure 3] or *Graham and Cairns* [2013b, Figures 4a], reveals quasi-regular and long structures of wave modulation. At higher velocity $v_S \simeq 0.6v_T$, one recovers typical waveforms as those observed by *Graham and Cairns* [2013b, Figure 19a] or *Malaspina et al.* [2010, Figure 1b], for example. For other conditions of observation but with the same velocity $v_S \simeq 0.6v_T$ (Figure 11), the observed waveform is very similar to those presented in *Malaspina et al.* [2011, Figure 2a] and *Graham et al.* [2012, Figure 2b]. So for small Δn, the waves are forming dense and packed sets of bursts with modulation features presenting

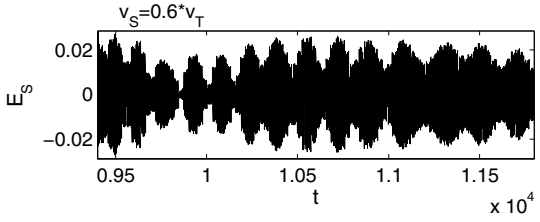

Figure 9. Waveform observed at $v_S = 0.6v_T$ for the same conditions as in Figures 8a–8d but with $z_S = 17,300\lambda_D$ at time $\omega_p t = 9400$. Physical parameters are the same as in Figure 8.

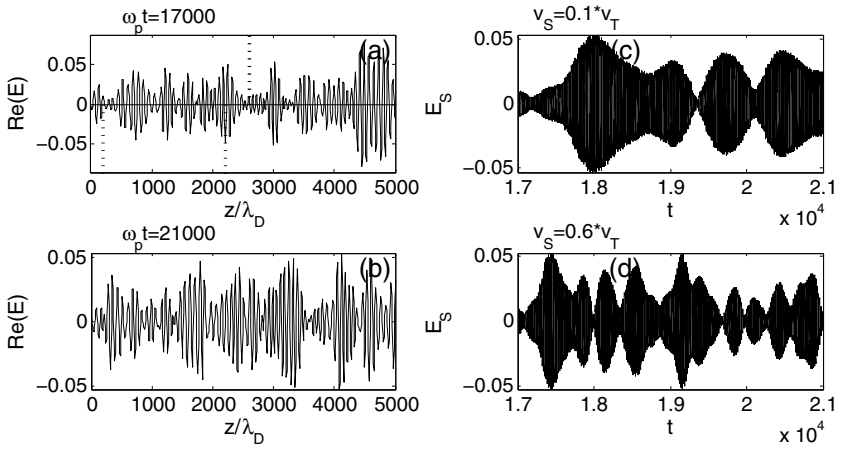

Figure 10. (a and b) Instantaneous electric field profiles at times $\omega_p t = 17,000$ and $\omega_p t = 21,000$, within the subbox $[L_{\min}, L_{\max}] = [0, 7000]$. (c and d) Corresponding waveforms which would be observed by a satellite moving at the velocities v_S and starting at $z_S = 2600\lambda_D$ (upward vertical line) at time $\omega_p t = 17,000$; the final positions of the satellite moving at the velocities $v_S = 0.1v_T$ (Figure 10c) and $v_S = 0.6v_T$ (Figure 10d) are marked by downward vertical lines. Main parameters are the following: $n_b/n_0 = 5\ 10^{-5}$, $v_b = 14v_T$, and $\Delta n \simeq 0.001$.

strong similitudes with waveforms captured in the solar wind. Moreover, they propagate with close velocities during rather long times and without significant variations of their shapes, as shown by Figure 12 which presents the wave energy profile $|E|^2$ as a function of time and space as well as cross sections at three selected times. When Δn is small, the waves' phases remain correlated during all the beam relaxation stage, explaining why long living clumped wave packets can be formed.

When Δn is sufficiently small, instantaneous as well as observed wave packets are not separated each other, i.e., one packet arrives at some point z just after another one, so that particles are able to interact with waves at any time t and any point z. The modulation of the wave packets is due to interference processes between waves and not to the presence of density inhomogeneities; indeed, when $\Delta n \gtrsim 0.01$, propagating wave packets can be separated one from another by several thousands of Debye lengths, so that particles are able to interact with waves only during short lapses of time, and the nature of the physical processes responsible for the modulation of the wave packets differs essentially from the case when $\Delta n \ll 0.01$.

Finally, Figure 13 shows the case of bursty instantaneous and observed waveforms in a plasma with density inhomogeneities of large amplitudes, $\Delta n \simeq 0.04$, for a satellite of velocity $v_S \simeq 0.15v_T$ moving within a large interval of time around $15,000\omega_p^{-1}$ (compare also with *Graham and Cairns* [2013b, Figure 19b]). Such waveforms are characteristic of cases when the solar wind plasma presents strong density inhomogeneities.

3. Discussion and Conclusion

Several conclusions can be inferred examining the waveforms produced in various simulations performed with different beam and plasma parameters typical for type III bursts, and comparing them to relevant events measured by the STEREO/TDS or the Wind spacecraft (see *stereo.gsfc.nasa.gov* and *wind.nasa.gov,* as well as the above cited papers). In this view, let us present in Figure 14 some waveforms measured in the solar wind with high time resolution by the WAVES (the Radio and Plasma Wave Investigation on the WIND Spacecraft) instrument onboard the Wind satellite [*Bougeret et al.*, 1995], in the electron foreshock region rather close to the tangential line where the electron distributions have quite a lot in common with the electron distributions in the solar wind during type III bursts (see *Bale et al.* [2000] for more details). One can see that they are qualitatively very similar

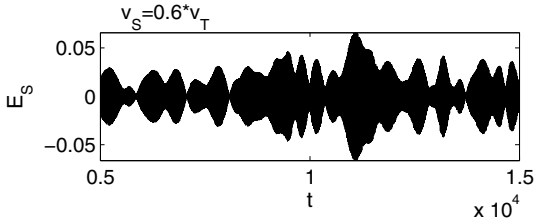

Figure 11. Waveform observed at $v_S = 0.6v_T$ for the same conditions as Figures 10a–10d but with $5000 < \omega_p t < 15,000$ and $z_S = 6900\lambda_D$. Physical parameters are the same as in Figure 10.

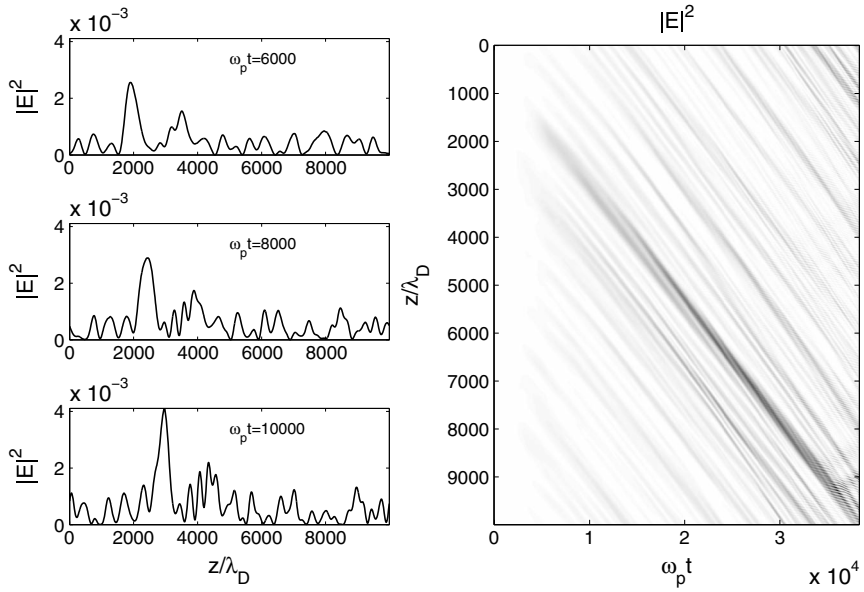

Figure 12. Wave energy profile $|E|^2$ as a function of time and space with three cross sections at the selected times $\omega_p t = 6000$, 8000, and 10,000. Parameters are the same as in Figure 10.

to waveforms or parts of waveforms obtained in our above simulations. For example, Figure 14a reproduces a part of the waveform of Figure 5c and is similar to that of Figure 9; Figures 14b and 14c have strong similarities with Figures 7c, 10, and Figure 14d which are analogous to Figure 6a. Moreover, it is possible, using our simulations, to reproduce with a very good accuracy the waveforms observed by the Wind satellite in Figure 14 (taking into account that the Langmuir waves and the solar wind propagate in inverse directions, contrary to the case of type III solar bursts), but our aim is only to show that the model and the simulations are able to account for the qualitative features of the observations of wave turbulence in the solar wind.

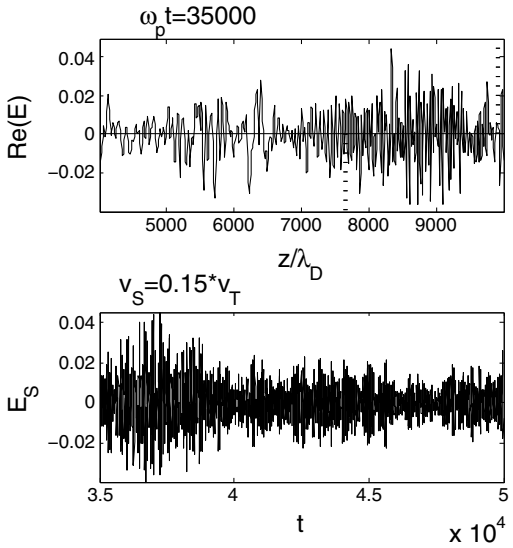

Figure 13. (top) Instantaneous electric field profile at time $\omega_p t = 35,000$. (bottom) Corresponding waveform which would be observed by a satellite moving at velocity $v_S = 0.15 v_T$ and starting at $z_S = 9900 \lambda_D$ (upward dotted vertical line in Figure 13 (top)) at time $\omega_p t = 35,000$; the final position of the satellite is marked by a downward dotted vertical line in Figure 13 (top). Main parameters are the following: $n_b/n_0 = 5\ 10^{-5}$, $v_b = 14 v_T$, and $\Delta n \simeq 0.04$, with $[L_{\min}, L_{\max}] = [4000, 10,000]$.

On the basis of our study, one can conclude that our calculations well agree with the most recent space measurements. We are able to reproduce all the salient characteristics of the observed wave packets and, in particular, the variety in their waveforms. First, the calculated waveforms appear as highly modulated wave packets which reproduce many characteristics of those observed by the space experiments: trains of clumps of various shapes, lengths, and amplitudes, isolated and localized packets, "smooth" modulations or more bursty ones with low-frequency modulations, waveforms presenting more or less regular or randomly shaped clumps. Then, the main cause of the clumping processes shaping the wave packets is likely the existence of randomly fluctuating density inhomogeneities. One observes also that most of the waveforms present rather complex sequences of bursts—and much more rarely only single or double

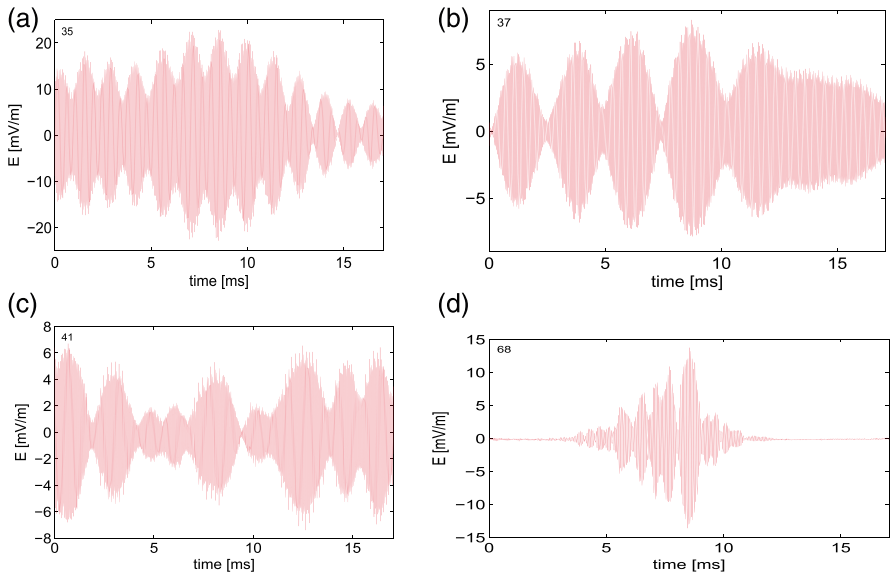

Figure 14. (a–d) Waveforms measured at 20 April 1996 by the Wind satellite in the electron foreshock region rather close to the tangential line where electron distributions have quite a lot in common with the electron distributions in the solar wind during type III bursts (see also *Bale et al.* [2000] for more details); the amplitude E of the electric field envelope (in mV/m) is displayed as a function of the time t in ms.

humps—and that waves are rather rarely trapped in density fluctuations, this occurring mainly when the average amplitude of density inhomogeneities is high (roughly $\Delta n \gtrsim 0.05$).

The organization of the waveforms into focused packets begins at early stages of the system's evolution, even before the growth of waves due to beam instability has reached an appreciable strength, indicating that nonlinear kinematic effects involving scattering and reflection are playing a significant role. No phenomena such as collapse or modulational instability are observed for the parameters used and the ponderomotive effects are shown to be weak, supposed that the beam density is sufficiently weak (what is the case here, see parameters above). As a consequence, many characteristic features of the wave packets' modulation are visible even in the absence of nonlinear effects such as wave-wave coupling, modulational instability, and collapse; the nonlinear processes are not the cause of the clumpy nature of the waveforms. However, they can modify them and even enhance the focusing processes which are shaping them (this topics will be discussed in detail in a forthcoming paper).

It is likely that the observation of highly localized and isolated wave packets is possible only if Δn exceeds some threshold. Moreover, the authors believe that the observation of such structures can be a signature for the presence of nonnegligible (but also not too high) levels of density fluctuations, i.e., $\Delta n \sim 0.01$. We also see that variations of the solar wind speed do not modify essentially the characteristic features of the observed waveforms reconstructed using the instantaneous profiles.

The authors believe that the clumping processes observed should be mainly due to nonlinear kinematic effects of wave propagation, reflection, and scattering in randomly fluctuating density profiles, which are influenced by the beam instability during the stage of linear wave growth. The wave spectra show that, during the evolution, reflected waves are generated after some time (see, e.g., Figure 4) and that the wave energy has tendency to focus near the wells' reflection points (see Figure 1b). This focusing is shown to occur with and without the beam, but it can be enhanced by the presence of the beam. Indeed, the beam instability plays an important role; after waves with resonant velocities $v_\varphi = \omega_k/k < v_b$ have gained energy from the beam particles with velocities $v < v_b$ via the beam instability developing at $\partial f/\partial v > 0$, they can transfer part of their energy to waves with $v_\varphi > v_b$, as a result of their scattering by the density inhomogeneities, the random modification of their phase velocities and their resonance conditions with the beam electrons. When Δn is sufficiently large ($\Delta n \gtrsim \alpha k^2 \lambda_D^2 \sim 0.01$ *Krafft et al.* [2013]), the Langmuir spectrum is flattened in the asymptotic stage. It is not the case when Δn is very small ($\Delta n \ll \alpha k^2 \lambda_D^2$ *Krafft et al.* [2013]).

In their turn, these waves can be submitted to Landau damping and thus transfer part of their energy to accelerate particles with velocities $v > v_b$. During these processes, the effective growth rate of each wave is changed randomly, and this organizes the modulation of the waveforms and modifies the number, the shapes, and the distribution of the clumps along the profiles. The combinations of all the mentioned effects contribute to create various types of modulations of the wave packet, its clumpiness indicating how the wave energy is distributed and more or less concentrated in localized spatial regions.

However, modulation effects shaping the Langmuir packets appear also in the presence of very small average levels of density inhomogeneities as the result of beatings between waves. Note also that other effects can influence the modulation effects structuring the waveforms: resonant wave-wave coupling between Langmuir wave packets and low-frequency (ion acoustic) waves, modulational instability where ponderomotive effects are strong, and collapse effects with further breaking into trains of ion acoustic solitons. The first one will be discussed in a forthcoming paper, particularly its influence on the modulation of the wave packets. The two other effects are usually not present in our simulations, taking into account the parameters chosen, so that their impact is not determinant on the focusing processes observed in our conditions; indeed, the presence of inhomogeneities decreases the maximum of wave energy reached which is thus decreasing below the modulational instability and collapse thresholds.

Appendix A: Theoretical Model

The 1-D theoretical model describes the self-consistent interaction of Langmuir waves with electron beams in plasmas with randomly varying density inhomogeneities. The dynamics of Langmuir and ion sound waves is calculated using the two Zakharov's equations [*Zakharov*, 1972] where a source term is added to model the beam. As shown in a previous paper [*Krafft et al.*, 2013], these equations can be written as

$$i\frac{\partial E}{\partial t} + \frac{3\lambda_D^2}{2}\omega_p\frac{\partial^2 E}{\partial z^2} - \omega_p\frac{\delta n}{2n_0}E = 4\pi i e n_b \sum_k \frac{\omega_p}{k}\frac{1}{N}\sum_p e^{i\omega_p t - ikz_p}e^{ikz}, \tag{A1}$$

$$\left(\frac{\partial^2}{\partial t^2} - c_s^2\frac{\partial^2}{\partial z^2}\right)\frac{\delta n}{n_0} = \frac{\partial^2}{\partial z^2}\frac{|E|^2}{16\pi m_i n_0}, \tag{A2}$$

where z is the coordinate along the ambient magnetic field $\mathbf{B}_0$; ω_p and λ_D are the electron plasma frequency and Debye length; k is the wave number of the Langmuir wave of frequency $\omega_k \simeq \omega_p + 3\omega_p k^2\lambda_D^2/2$; $\mathcal{E} = \mathrm{Re}(E(z,t)\,e^{-i\omega_p t})$ is the electric field, and $E(z,t)$ is its slowly varying envelope; δn is the low-frequency density perturbation; m_i and m_e are the ion and electron masses; $-e < 0$ is the electron charge; n_b is the beam density; T_i and T_e are the ion and electron temperatures, which are supposed to satisfy the condition $T_i \ll T_e$; $c_s = \sqrt{(T_e + 3T_i)/m_i}$ is the ion acoustic velocity; z_p is the position of the particle p; and N is the number of macroparticles, i.e., the number of resonant electrons.

The model divides the total particle distribution in two groups: (i) the background plasma whose particles interact nonresonantly with the waves, and (ii) the beam particles which exchange resonantly with the waves significant amounts of energy and momentum [e.g., *O'Neil et al.*, 1971; *Volokitin and Krafft*, 2004; *Zaslavsky et al.*, 2006; *Krafft et al.*, 2005, 2006; *Krafft and Volokitin*, 2010; *Krafft et al.*, 2010; *Zaslavsky et al.*, 2007; *Krafft and Volokitin*, 2013]. The first group of electrons supports the wave dispersion and its dynamics is modeled using the dielectric constant in the frame of a linear approach (see also the beam source term in (A1)). On another hand, the resonant electrons of velocity v exchange momentum and energy with the plasma waves at the Landau resonances $\omega_k \simeq \omega_p \simeq kv$. Their dynamics is calculated by solving the Newton equations. Such approach leads to a drastic reduction of the number of macroparticles required in the calculations, giving the possibility to study the microscopic beam dynamics and the Langmuir turbulence over long periods of time. Nevertheless, it is required the resonant particles' density n_b to be much less than the ambient plasma density, i.e., $n_b \ll n_0$.

The Newton equations for the N particles p have to be added to equations (A1) and (A2)

$$m_e\frac{\mathrm{d}v_p}{\mathrm{d}t} = -e\mathcal{E}(z_p,t) = -e\,\mathrm{Re}\left(\sum_k E_k e^{ikz_p - i\omega_k t}\right), \quad \frac{\mathrm{d}z_p}{\mathrm{d}t} = v_p, \tag{A3}$$

where v_p is the velocity of the electron p; E_k is the Fourier component of E

$$E_k(t) = \int_0^L E(z,t)e^{-ikz}\frac{dz}{L},$$

where $L = N/n_b$ is the size of the system. Rewriting equation (A1) in the k space, one obtains that

$$i\left(\frac{\partial}{\partial t} - \gamma_k^{(e)}\right)E_k = \frac{3}{2}\omega_p k^2 \lambda_D^2 E_k + \frac{\omega_p}{2}(\rho E)_k + i\frac{4\pi e\omega_p n_b}{k}J_k, \quad \text{(A4)}$$

where $\rho = \delta n/n_0$; a kinetic damping factor $\gamma_k^{(e)} = -\mathrm{Im}\varepsilon_k^{(e)}/(\partial \mathrm{Re}\varepsilon_k^{(e)}/\partial\omega_k)$ (where the superscript (e) refers to electrons) is added eventually in (A4) in order to take into account the damping of the plasma waves when interacting with thermal particles or with nonthermal electrons of the background plasma distribution, as for example non-Maxwellian tails.

The Fourier transforms of equation (A2) and of the plasma continuity equation lead to the following expressions (ion damping is not included)

$$\frac{\partial}{\partial t}\rho_k = ikc_s u_k, \quad \text{(A5)}$$

$$\frac{\partial u_k}{\partial t} = ikc_s\left(\rho_k + \frac{(|E|^2)_k}{16\pi m_i n_0 c_s^2}\right), \quad \text{(A6)}$$

where v_i and $u = v_i/c_s$ are the ion velocity and its normalized value. Equations (A4)–(A6) together with equation (A3) form the complete set of equations of our model.

References

Acknowledgments
We thank T. Dudok de Wit (ddwit@cnrs-orleans.fr) and V. Krasnoselskikh (vkrasnos@gmail.com) for providing the data of Figure 14, available at wind.nasa.gov. V.K. acknowledges the financial support of the Centre National d'Etudes Spatiales (CNES) through the grant "Invited scientist STEREO S/WAVES." This work was granted access to the HPC resources of IDRIS under the allocation 2013-i2013057017 made by GENCI. This work has been done within the LABEX Plas@par project and received financial state aid managed by the Agence Nationale de la Recherche, as part of the programme "Investissements d'avenir" under the reference ANR-11-IDEX-0004-02. C.K. acknowledges the "Programme National Soleil Terre" (PNST) and the Centre National d'Etudes Spatiales (CNES, France).

Michael Balikhin thanks the reviewers for their assistance in evaluating this paper.

Bale, S. D., D. E. Larson, R. P. Lin, P. J. Kellogg, K. Goetz, and S. J. Monson (2000), On the beam speed and wavenumber of intense electron plasma waves near the foreshock edge, *J. Geophys. Res.*, *105*(A12), 27,353–27,367, doi:10.1029/2000JA900042.

Bonnell, J., P. Kintner, J.-E. Wahlund, and J. A. Holtet (1997), Modulated Langmuir waves: Observations from Freja and Scifer, *J. Geophys. Res.*, *102*(A8), 17,233–17,240, doi:10.1029/97JA01499.

Boshuizen, C. R., I. H. Cairns, and P. A. Robinson (2004), Electric field distributions for Langmuir waves in planetary foreshocks, *J. Geophys. Res.*, *109*, A08101, doi:10.1029/2004JA010408.

Bougeret, J.-L., et al. (1995), WAVES: The radio and plasma wave investigation on the WIND spacecraft, *Space Sci. Rev.*, *71*, 231–263, doi:10.1007/BF00751331.

Bougeret, J.-L., et al. (2008), S/waves: The radio and plasma wave investigation on the Stereo mission, *Space Sci. Rev.*, *136*, 487–529, doi:10.1007/s11214-007-9298-8.

Celnikier, L. M., C. C. Harvey, R. Jegou, P. Moricet, and M. Kemp (1983), A determination of the electron density fluctuation spectrum in the solar wind, using the ISEE propagation experiment, *Astron. Astrophys.*, *126*, 293–298.

Celnikier, L. M., L. Muschietti, and M. V. Goldman (1987), Aspects of interplanetary plasma turbulence, *Astron. Astrophys.*, *181*, 138–154.

Ergun, R. E., et al. (1998), Wind spacecraft observations of solar impulsive electron events associated with solar type III radio bursts, *Astrophys. J.*, *503*(1), 435–445, doi:10.1086/305954.

Ergun, R. E., et al. (2008), Eigenmode structure in solar-wind Langmuir waves, *Phys. Rev. Lett.*, *101*, 051,101, doi:10.1103/PhysRevLett.101.051101.

Ginzburg, V., and V. Zheleznyakov (1958), On possible mechanisms of sporadic solar radio emission, *Sov. Astron. AJ*, *2*, 653–668.

Graham, D. B., and I. H. Cairns (2013a), Constraints on the formation and structure of Langmuir eigenmodes in the solar wind, *Phys. Rev. Lett.*, *111*, 121,101, doi:10.1103/PhysRevLett.111.121101.

Graham, D. B., and I. H. Cairns (2013b), Electrostatic decay of Langmuir/z-mode waves in type III solar radio bursts, *J. Geophys. Res. Space Physics*, *118*, 3968–3984, doi:10.1002/jgra.50402.

Graham, D. B., I. H. Cairns, D. R. Prabhakar, R. E. Ergun, D. M. Malaspina, S. D. Bale, K. Goetz, and P. J. Kellogg (2012), Do Langmuir wave packets in the solar wind collapse?, *J. Geophys. Res.*, *117*, A09107, doi:10.1029/2012JA018033.

Gurnett, D., and R. Anderson (1976), Electron plasma oscillations associated with type III radio bursts, *Science*, *194*(4270), 1159–1162, doi:10.1126/science.194.4270.1159.

Gurnett, D., G. Hospodarsky, W. Kurth, D. Williams, and S. Bolton (1993), Fine structure of Langmuir waves produced by a solar electron event, *J. Geophys. Res.*, *98*(A4), 5631–5637, doi:10.1029/92JA02838.

Gurnett, D. A., R. R. Anderson, F. L. Scarf, and W. S. Kurth (1978), The heliocentric radial variation of plasma oscillations associated with type III radio bursts, *J. Geophys. Res.*, *83*, 4147–4152, doi:10.1029/JA083iA09p04147.

Gurnett, D. A., J. E. Maggs, D. L. Gallagher, W. S. Kurth, and F. L. Scarf (1981), Parametric interaction and spatial collapse of beam-driven Langmuir waves in the solar wind, *J. Geophys. Res.*, *86*(A10), 8833–8841, doi:10.1029/JA086iA10p08833.

Gurnett, D. A., W. S. Kurth, R. R. Shaw, A. Roux, R. Gendrin, C. F. Kennel, F. L. Scarf, and S. D. Shawhan (1992), The Galileo plasma wave investigation, *Space Sci. Rev.*, *60*, 341–355, doi:10.1007/BF00216861.

Henri, P., C. Briand, A. Mangeney, S. D. Bale, F. Califano, K. Goetz, and M. Kaiser (2009), Evidence for wave coupling in type III emissions, *J. Geophys. Res.*, *114*, A03103, doi:10.1029/2008JA013738.

Hess, S. L. G., D. M. Malaspina, and R. E. Ergun (2011), Size and amplitude of Langmuir waves in the solar wind, *J. Geophys. Res.*, *116*, A07104, doi:10.1029/2010JA016163.

Hospodarsky, G., and D. Gurnett (1995), Beat-type Langmuir wave emissions associated with a type III solar radio bursts, *Geophys. Res. Lett.*, *22*, 1161–1164, doi:10.1029/95GL00303.

Kellogg, P., K. Goetz, S. Monson, and S. Bale (1999), Langmuir waves in a fluctuating solar wind, *J. Geophys. Res.*, *104*(A8), 17069–17078, doi:10.1029/1999JA900163.
Kellogg, P. J. (1986), Observations concerning the generation and propagation of type III solar bursts, *Astron. Astrophys.*, *169*, 329–335.
Kellogg, P. J., and T. S. Horbury (2005), Rapid density fluctuations in the solar wind, *Ann. Geophys.*, *23*, 3765–3773, doi:10.5194/angeo-23-3765-2005.
Kellogg, P. J., K. Goetz, S. J. Monson, S. D. Bale, M. J. Reiner, and M. Maksimovic (2009), Plasma wave measurements with STEREO S/WAVES: Calibration, potential model, and preliminary results, *J. Geophys. Res.*, *114*, A02107, doi:10.1029/2008JA013566.
Kojima, H., H. Furuya, H. Usui, and H. Matsumoto (1997), Modulated electron plasma waves observed in the tail lobe: Geotail waveform observations, *Geophys. Res. Lett.*, *24*, 3049–3052, doi:10.1029/97GL03043.
Krafft, C., and A. Volokitin (2006), Stabilization of the fan instability: Electron flux relaxation, *Phys. Plasmas*, *13*, 122,301, doi:10.1063/1.2372464.
Krafft, C., and A. Volokitin (2010), Nonlinear fan instability of electromagnetic waves, *Phys. Plasmas*, *17*, 102,303, doi:10.1063/1.3479829.
Krafft, C., and A. Volokitin (2013), Nonturbulent stabilization of ion fluxes by the fan instability, *Phys. Lett. A*, *377*, 1189–1198, doi:10.1016/j.physleta.2013.03.011.
Krafft, C., A. Volokitin, and A. Zaslavsky (2005), Saturation of the fan instability: Nonlinear merging of resonances, *Phys. Plasmas*, *12*, 112309, doi:10.1063/1.2118727.
Krafft, C., A. Volokitin, and A. Zaslavsky (2010), Nonlinear dynamics of resonant interactions between wave packets and particle distributions with loss cone-like structures, *Phys. Rev. E*, *82*(6), 066402, doi:10.1103/PhysRevE.82.066402.
Krafft, C., A. S. Volokitin, and V. V. Krasnoselskikh (2013), Interaction of energetic particles with waves in strongly inhomogeneous solar wind plasmas, *Astrophys. J.*, *778*, 111, doi:10.1088/0004-637X/778/2/111.
Krasnoselskikh, V., V. V. Lobzin, K. Musatenko, J. Soucek, J. S. Pickett, and I. H. Cairns (2007), Beam-plasma interaction in randomly inhomogeneous plasmas and statistical properties of small-amplitude Langmuir waves in the solar wind and electron foreshock, *J. Geophys. Res.*, *112*, A10109, doi:10.1029/2006JA012212.
Lin, R., W. Levedahl, W. Lotko, D. Gurnett, and F. Scarf (1986), Evidence for nonlinear wave-wave interaction in solar type III radio bursts, *Astrophys. J.*, *308*, 954–965, doi:10.1086/164563.
Lin, R. P., D. W. Potter, D. A. Gurnett, and F. L. Scarf (1981), Energetic electrons and plasma waves associated with a solar type III radio burst, *Astrophys. J.*, *251*, 364–373, doi:10.1086/159471.
Malaspina, D. M., and R. E. Ergun (2008), Observations of three-dimensional Langmuir wave structure, *J. Geophys. Res.*, *113*, A12108, doi:10.1029/2008JA013656.
Malaspina, D. M., P. J. Kellogg, S. D. Bale, and R. E. Ergun (2010), Measurements of rapid density fluctuations in the solar wind, *Astrophys. J.*, *711*, 322–327, doi:10.1088/0004-637X/711/1/322.
Malaspina, D. M., I. H. Cairns, and R. E. Ergun (2011), Dependence of Langmuir wave polarization on electron beam speed in type III solar radio bursts, *Geophys. Res. Lett.*, *38*, L13101, doi:10.1029/2011GL047642.
Mangeney, A., C. Salem, C. Lacombe, J. L. Bougeret, C. Perche, R. Manning, P. J. Kellogg, K. Goetz, S. J. Monson, and J.-M. Bosqued (1999), Wind observations of coherent electrostatic waves in the solar wind, *Ann. Geophys.*, *17*, 307–320, doi:10.1007/s00585-999-0307-y.
Melrose, D. B., G. A. Dulk, and I. H. Cairns (1986), Clumpy Langmuir waves in type III solar radio bursts, *Astron. Astrophys.*, *163*, 229–238.
Muschietti, L., I. Roth, and R. Ergun (1994), Interaction of Langmuir wave packets with streaming electrons: Phase-correlation aspects, *Phys. Plasmas*, *1*, 1008–1024, doi:10.1063/1.870781.
Muschietti, L., I. Roth, and R. E. Ergun (1995), Kinetic localization of beam-driven Langmuir waves, *J. Geophys. Res.*, *100*(A9), 17,481–17,490, doi:10.1029/95JA00595.
Nicholson, D. R., M. V. Goldman, P. Hoyng, and J. C. Weatherall (1978), Nonlinear Langmuir waves during type III solar radio bursts, *Astrophys. J.*, *223*, 605–619, doi:10.1086/156296.
Nulsen, A. L., I. H. Cairns, and P. A. Robinson (2007), Field distributions and shapes of Langmuir wave packets observed by Ulysses in an interplanetary type III burst source region, *J. Geophys. Res.*, *112*, A05107, doi:10.1029/2006JA011873.
O'Neil, T., J. Winfrey, and J. Malmberg (1971), Nonlinear interaction of a small cold beam and a plasma, *Phys. Fluids*, *14*, 1204–1212.
Robinson, P. A. (1992), Clumpy Langmuir waves in type III radio sources, *Solar Phys.*, *139*, 147–163, doi:10.1007/BF00147886.
Robinson, P. A., A. J. Willes, and I. H. Cairns (1993), Dynamics of Langmuir and ion-sound waves in type III solar radio sources, *Astrophys. J.*, *408*, 720–734, doi:10.1086/172632.
Smith, D. F., and D. Sime (1979), Origin of plasma-wave clumping in type III solar radio burst sources, *Astrophys. J.*, *233*, 998–1004, doi:10.1086/157463.
Souček, J., V. Krasnoselskikh, T. D. de Wit, J. Pickett, and C. Kletzing (2005), Nonlinear decay of foreshock Langmuir waves in the presence of plasma inhomogeneities: Theory and Cluster observations, *J. Geophys. Res.*, *110*, A08102, doi:10.1029/2004JA010977.
Thejappa, G., R. J. MacDowall, E. E. Scime, and J. E. Littleton (2003), Evidence for electrostatic decay in the solar wind at 5.2 au, *J. Geophys. Res.*, *108*, A31139, doi:10.1029/2002JA009290.
Volokitin, A., and C. Krafft (2004), Interaction of suprathermal electron fluxes with lower hybrid waves, *Phys. Plasmas*, *11*(6), 3165–3176, doi:10.1063/1.1715100.
Volokitin, A., and C. Krafft (2012), Velocity diffusion in plasma waves excited by electron beams: A numerical experiment, *Plasma Phys. Contr. Fusion*, *54*(085002), doi:10.1088/0741-3335/54/8/085002.
Volokitin, A., V. Krasnoselskikh, C. Krafft, and E. Kuznetsov (2013), Modelling of the beam-plasma interaction in a strongly inhomogeneous plasma, *AIP Conf. Proc.*, *1539*(1), 78–81, doi:10.1063/1.4810994.
Zakharov, V. (1972), Collapse of Langmuir waves, *Sov. Phys. JETP*, *35*(5), 908–914.
Zaslavsky, A., C. Krafft, and A. Volokitin (2006), Stochastic processes of particle trapping and detrapping by a wave in a magnetized plasma, *Phys. Rev. E*, *73*(016406), doi:10.1103/PhysRevE.73.016406.
Zaslavsky, A., C. Krafft, and A. Volokitin (2007), Loss-cone instability: Wave saturation by particle trapping, *Phys. Plasmas*, *14*, 122302, doi:10.1063/1.2799621.
Zaslavsky, A., A. Volokitin, V. V. Krasnoselskikh, M. Maksimovic, and S. D. Bale (2010), Spatial localization of Langmuir waves generated from an electron beam propagating in an inhomogeneous plasma: Applications to the solar wind, *J. Geophys. Res.*, *115*, A08103, doi:10.1029/2009JA014996.